PHYSICAL REVIEW B **77**, 125106 (2008)

Importance of t_{2g}-e_g hybridization in transition metal oxides

Sylvain Landron and Marie-Bernadette Lepetit
CRISMAT, ENSICAEN-CNRS UMR6508, 6 boulevard Maréchal Juin, 14050 Caen, France

(Received 12 June 2007; revised manuscript received 2 October 2007; published 7 March 2008)

We studied the influence of the trigonal distortion of the regular octahedron along the (111) direction, as found in the CoO_2 layers. Under this distortion the t_{2g} orbitals split into one a_{1g} and two degenerate e'_g orbitals. We focused on the relative order of these orbitals. Using quantum chemical calculations of embedded clusters at different levels of theory, we analyzed the influence of the different effects not taken into account in crystalline field theory; that is, metal-ligand hybridization, the long-range crystalline field, screening effects, and orbital relaxation. We found that none of them is responsible for the relative order of the t_{2g} orbitals. In fact, the trigonal distortion allows a mixing of the t_{2g} and e_g orbitals of the metallic atom. This hybridization is at the origin of the a_{1g}-e'_g relative order and of the incorrect prediction of crystalline field theory.

DOI: 10.1103/PhysRevB.77.125106 PACS number(s): 71.70.Ch, 71.27.+a, 71.10.Fd

I. INTRODUCTION

Since the discovery of superconductivity in the hydrated $Na_{0.35}CoO_2 \cdot 1.3H_2O$ compound,[1] and of the very large thermopower[2] in the $Na_{0.7\pm\delta}CoO_2$ members of the same family, the interest of the community in systems built from CoO_2 layers has exploded. The first step in the understanding of the electronic properties of transition metal oxides, such as the CoO_2-based compounds, is the analysis of the crystalline field splitting of the d orbitals of the transition metal atom. Indeed, depending on this splitting, the spin state of the atom, the nature of the Fermi level orbitals, and thus the Fermi level properties will differ.

The CoO_2 layers are built from edge-sharing CoO_6 octahedra (see Fig. 1). In these layers, the first coordination shell of the metal atom differs from the regular octahedron by a trigonal distortion along the threefold (111) axis (see Fig. 2). In all known materials (whether cobalt oxides or other metal oxides such as $LiVO_2$, $NaTiO_2$, $NaCrO_2$, etc.), this distortion is in fact a compression. The local symmetry group of the metal atom is lowered from O_h to D_{3d}. The T_{2g} irreducible representation of the O_h group is thus split into one E_g and one A_{1g} representation. The relative energy of the resulting e'_g and a_{1g} orbitals (see Fig. 2) has been a subject of controversy in the recent literature, as far as the low-spin Co^{4+} ion is concerned. At this point let us point out the crucial importance of the knowledge of this energetic order for the understanding of the low-energy properties of the CoO_2 layers. Indeed, the possible existence of orbital order, as well as the minimal model pertinent for the description of these systems, depend on this order.

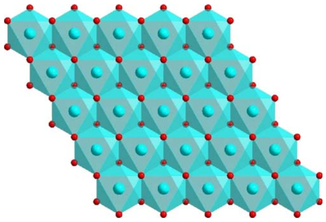

FIG. 1. (Color online) Schematic representation of the CoO_2 layers.

Authors such as Kashibae and Maekawa,[3] following crystalline field theory, support the idea that the a_{1g} orbital is of lower energy than the two degenerate e'_g orbitals, leading to an orbital degeneracy for the Co^{4+} ion. On the contrary, *ab initio* quantum chemical calculations for strongly correlated systems[6] yield an a_{1g} orbital of higher energy than the e'_g orbitals, and a nondegenerate Fermi level of the Co^{4+} ion. As far as density functional methods are concerned, some authors[4] find the a_{1g} orbital of higher energy than the e'_g, while others[5] find the reverse order (see Fig. 2).

Angle-resolved photoemission spectroscopy (ARPES) experiments were performed on several CoO_2 compounds.[7] This technique probes the Fermi surface, and clearly shows that the Fermi surface of the CoO_2 layers issues from the a_{1g} orbitals, and not at all from the e'_g orbitals (orbitals of E_g symmetry, coming from the former t_{2g} orbitals), supporting the *ab initio* results.

In the present work, we will try to understand the reasons why the crystalline field model is unable to find the correct energetic order of t_{2g} orbitals in such trigonal distortions. Several hypotheses can be made to explain the orbital order:

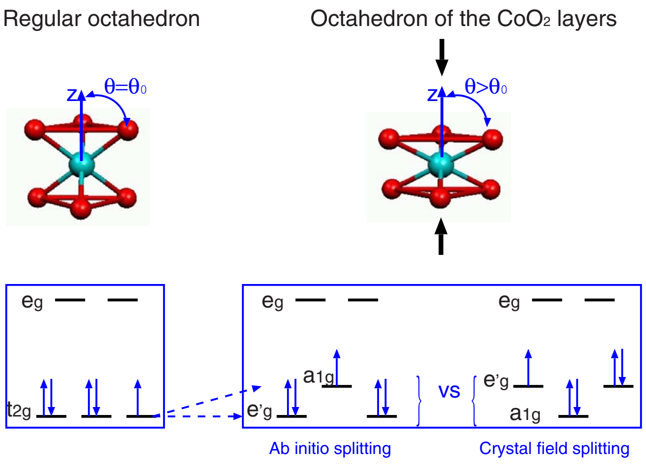

FIG. 2. (Color online) Schematic representation of cobalt $3d$ splitting. θ represents the angle between the $\mathbf{z}$ axis—the threefold (111) axis of the CoO_6 octahedron—and the Co-O direction. $\theta_0 = \arccos(1/\sqrt{3}) \simeq 54.74°$ is the θ angle for the regular octahedron.

1098-0121/2008/77(12)/125106(8)

the delocalization of the metal $3d$ orbitals toward the ligands, the fact that the electrostatic potential of the whole crystal differs from the one assumed in the crystalline field model, correlation effects within the $3d$ shell, screening effects, etc. All these hypotheses will be specifically tested on the Co^{4+} ($3d^5$) ion that is subject in this work to a more thorough study than other metal d-orbital fillings. Nevertheless, other metal fillings ($3d^1$–$3d^3$, which can be found in vanadium, titanium, and chromium oxides) will also be studied. We will see the crucial importance of the band filling on the t_{2g} orbital order. In this work we will focus only on the O_h to D_{3d} trigonal distortion, the subject of the controversy.

The next section will present the method used in this work, Secs. III and IV will report the calculations and analyze them, and finally the last section will be devoted to the conclusions.

II. COMPUTATIONAL METHOD AND DETAILS

The energy of the atomic $3d$ orbitals is an essentially local value, as supposed in the crystalline field model. However, its analysis exhibits some nonlocal contributions. Indeed, orbitals energies can be seen as resulting from the following terms: the electrostatic potential due to the first coordination shell—in the present case, the six oxygen atoms of the octahedron, further referred as nearest-neighbor oxygens (NNOs); the electrostatic potential due to the rest of the crystal; the kinetic energy, which includes the hybridization of the metal orbitals with nearest-neighbor ligands; the Coulomb and exchange contributions within the $3d$ shell; the radial relaxation of the $3d$ orbitals; and finally the virtual excitations from the other orbitals that are responsible for the screening effects. All these contributions, except for the electrostatic potential due to the rest of the crystal (nuclear attractions and Coulomb interactions), are essentially local contributions[8] and known to decrease very rapidly with increasing distance from the metal atom. In fact, they are mostly restricted to the first coordination shell of cobalt. In contrast, the Madelung potential retains the nonlocal contributions resulting from the nuclear attraction and the Coulomb electron-electron repulsion. It is known to be very slowly convergent with the distance. We thus made calculations at different levels, including first all the above effects, and then excluding them one at the time, in order to end up with only the effects included in the crystalline field model.

The calculations will thus be done on CoO_6 or Co fragments. Different embeddings and different levels of calculation will be used. The Co-O distance will be fixed to the value of the superconducing compound, i.e., $R_{\text{Co-O}} = 1.855$ Å. The angle θ between the Co-O direction and the $\mathbf{z}$ axis (see Fig. 2 above) will be varied from 0 to 90°.

The calculations will be done at the level of the complete active space self-consistent field+difference dedicated configuration interaction[9,10] (CASSCF+DDCI; see Sec. II A) for the most involved case, using the core pseudopotential and basis set of Barandiaran *et al.*[11] The fragment used will include all the first coordination oxygens in addition to the cobalt atom. The embedding will be designed so as to properly represent the full Madelung potential of the superconducting material, and the exclusion effects of the rest of the crystal on the computed fragment electrons (see Ref. 6 for further details). For the simplest case a minimal basis set derived from the preceding one will be used, and only the cobalt atom will be included in the computed fragment. The effect of the crystalline field will be described by -2 point charges located at the positions of the first coordination shell oxygens. The calculations will be done at the CASSCF level only. Between these two extreme cases, several intermediate ones will be considered, in order to check the previously enumerated points.

The electrostatic potential due to the cobalt first oxygen neighbors, as well as the unscreened Coulomb and exchange contributions within the $3d$ shell, are included in all calculations. The electrostatic potential is treated either through the inclusion of the NNOs in the computed fragment or through -2 point charges. The Coulomb and exchange contributions are treated through the CASSCF calculation. The electrostatic contribution of the rest of the crystal is included only in the most involved calculations, using an appropriate embedding of point charges and a total ions pseudopotential.[12] The hybridization of the metal $3d$ orbitals is treated by including explicitly the NNOs in the considered fragment (CoO_6). The radial relaxation of the $3d$ orbitals is treated when extended basis sets are used. When a minimal basis set is used, the radial part of the orbitals is frozen as in the high-spin state of the isolated Co^{4+} ion. Finally, the screening effects are treated only when the calculation is performed at the CASSCF+DDCI level.

A. The CASSCF and DDCI methods

Let us now describe briefly the CASSCF and DDCI *ab initio* methods. These methods are configuration interaction (CI) methods, that is, exact diagonalization methods within a selected set of Slater determinants. These methods were specifically designed to treat strongly correlated systems, for which there is no qualitative single-determinant description. The CASSCF method treats exactly all correlation and exchange effects within a selected set of orbitals (here the $3d$ shell of the cobalt atom). The DDCI method treats in addition the excitations responsible for the screening effects on the exchange, repulsion, hopping, etc. integrals. These methods are based on the partitioning of the fragment orbitals into three sets: *the occupied orbitals*, which are always doubly occupied in all determinants of the complete active space (CAS) (here the cobalt inner electrons and the NNO ones), *the active orbitals*, which can have all possible occupations and spins in the CAS (here the cobalt $3d$ orbitals), and *the virtual orbitals*, which are always empty in the CAS.

The CASCI method is the exact diagonalization within the above-defined complete active space. The CASSCF method optimizes in addition the fragment orbitals in order to minimize the CASCI wave function energy. This is a mean-field method for the occupied orbitals but all the correlation effects within the active orbitals are taken into account. Finally the DDCI method uses a diagonalization space that includes the CAS and all single and double excitations on all determinants of the CAS, except the ones that excite two occupied orbitals into two virtual orbitals. Indeed, such excitations can be shown not to contribute—at the second order of perturbation—to the energy differences between states that differ essentially in their CAS wave function. Therefore, they have little importance for the present work. The DDCI method thus accurately treats both the correlation within the CAS and the screening effects.

Compared to the very popular density functional theory (DFT) methods, the CAS+DDCI method presents the advantage of treating exactly the correlation effects within the $3d$ shell. This is an important point for strongly correlated materials such as the present ones. Indeed, even if the DFT methods are supposed to be exact provided knowledge of the correct exchange-correlation functional, the present functionals work very well for weakly correlated systems, but encounter more difficulties with strong correlation effects. For instance the local density approximation (LDA) finds most of the sodium cobaltite compounds ferromagnetic, in contradiction with experimental results. LDA+U functionals try to correct these problems by using an *ad hoc* on-site repulsion U within the strongly correlated shells. This correction yields better results; however, it treats the effect of the repulsion within a mean-field approximation, still lacking a proper treatment of the strong correlation. The drawbacks of the CAS+DDCI method compared to the DFT methods are its cost in terms of CPU time and the necessity to work on formally finite and relatively small systems. In the present case, however, this drawback appears to be an advantage since it decouples the local quantities under consideration from the dispersion problem.

III. RESULTS AND ANALYSIS

Let us first attract the attention of the reader to what is supposed to be the energy difference between the e_g' and a_{1g} orbitals of the Co^{4+} ion in an effective model. In fact, the pertinent parameters for an effective model should be such that one can reproduce by their means the exact energies or, in the present case, the *ab initio* calculation of the different Co^{4+} atomic states. It turns out, that within a Hubbard-type model the pertinent effective orbital energies should obey the following set of equations:

$$E(|\mathbf{a_{1g}}\rangle) = 4\varepsilon(e_g') + \varepsilon(a_{1g}) + 2U + 8U' - 4J_H,$$

$$E(|\mathbf{e_g'}\rangle) = 3\varepsilon(e_g') + 2\varepsilon(a_{1g}) + 2U + 8U' - 4J_H,$$

$$\Delta E = E(|\mathbf{e_g'}\rangle) - E(|\mathbf{a_{1g}}\rangle) = \varepsilon(a_{1g}) - \varepsilon(e_g')$$

where the schematic picture of the $|\mathbf{e_g'}\rangle$ and $|\mathbf{a_{1g}}\rangle$ states is given in Fig. 3, $\varepsilon(e_g')$ and $\varepsilon(a_{1g})$ are the effective orbital energies of the e_g' and a_{1g} atomic orbitals, U is the effective electron-electron repulsion of two electrons in the same cobalt $3d$ orbital, U' the effective repulsion of two electrons in different cobalt $3d$ orbitals, and J_H the atomic Hund's exchange effective integrals within the cobalt $3d$ shell.

A. The reference calculation

The reference calculation includes all effects detailed in the preceding section. For the superconducting compound the effective t_{2g} splitting was reported in Ref. 6 to be

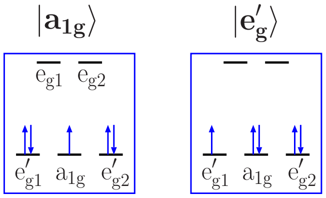

FIG. 3. (Color online) Schematic representation of the Co^{4+} states of interest. Let us point out that $|\mathbf{e_g'}\rangle$ is doubly degenerate, the hole being located either on the e_{g1}' or on the e_{g2}' orbitals.

$$\Delta E = \varepsilon(a_{1g}) - \varepsilon(e_g') = 315 \text{ meV}.$$

This point corresponds to $\theta \simeq 61.5°$ (which is a value of θ larger than that of the regular octahedron $\theta_0 \simeq 54.74°$) where the crystalline field theory predicts a reverse order between the t_{2g} orbitals.

B. Screening effects

The effect of the screening on the t_{2g} orbital splitting can be evaluated by doing a simple CASCI calculation using the same fragment, embedding, basis set, and orbitals as the preceding calculation. Without the screening effects, one finds a t_{2g} splitting of

$$\Delta E = \varepsilon(a_{1g}) - \varepsilon(e_g') = 428 \text{ meV}.$$

Obviously the screening effects cannot be taken as responsible for the qualitative energetic order between the a_{1g} and e_g' orbitals.

C. Cobalt $3d$–oxygen hybridization

The effect of the hybridization of the cobalt $3d$ orbitals with the neighboring oxygen ligands can be evaluated by taking out the oxygen atoms from the quantum cluster, and treating them as simple -2 point charges at the atomic locations. The other parameters of the calculation are kept as in the preceding case. The new orbitals are optimized at the average CASSCF level between the two $|\mathbf{e_g'}\rangle$ and the $|\mathbf{a_{1g}}\rangle$ states. It results in a t_{2g} splitting of

$$\Delta E = \varepsilon(a_{1g}) - \varepsilon(e_g') = 40 \text{ meV}$$

for the superconducting compound. Again the hybridization of the cobalt $3d$ orbitals with the neighboring oxygens cannot be taken as responsible for the inversion of the splitting between the a_{1g} and e_g' orbitals.

D. Long-range electrostatic potential

The effect of the long-range electrostatic potential can be evaluated by restricting the embedding to the NNO point charges only, that is, to the electrostatic potential considered in the crystalline field method. One finds a t_{2g} splitting of

$$\Delta E = \varepsilon(a_{1g}) - \varepsilon(e_g') = 124 \text{ meV}.$$

Once again, the result is positive and thus the long-range electrostatic potential is not the cause of the crystalline field inversion of the t_{2g} splitting.

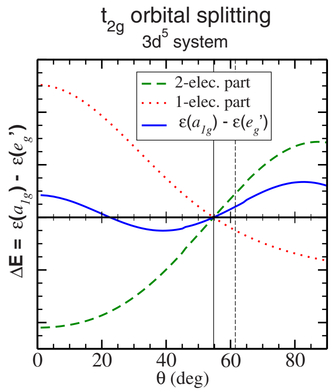

FIG. 4. (Color online) Orbital splitting between the a_{1g} and e_g' orbitals when only the nearest-neighbor ligand electrostatic field is included. The dotted red curve corresponds to the single-electron part of the orbital energy difference ΔE_1, that is, the kinetic energy [Eq. (1)], the electron-charge interaction [Eq. (2)], and the interaction with the core electrons [Eq. (3)]. The dashed green curve corresponds to the two-electron part of the orbital energy difference ΔE_2, that is, the repulsion and exchange terms within the $3d$ shell [Eq. (4)]. The solid vertical line indicates the regular octahedron θ value and the dashed vertical line the θ value for the superconducting compound.

E. Orbital radial relaxation

At this point only a few effects on top of the crystalline field theory are still treated in the calculation. One of them is the radial polarization effect of the $3d$ orbitals, which allows their adaptation to the different occupations in the specific $|\mathbf{a_{1g}}\rangle$ and $|\mathbf{e_g'}\rangle$ states. This polarization is due to the use of an extended basis set. We thus reduce the basis set to a minimal basis set [only one orbital degree of freedom per (n,l) occupied or partially occupied atomic shell]. The minimal basis set was obtained by the contraction of the extended one, the radial part of the orbitals being frozen as that of the isolated Co^{4+} high-spin state. This choice was done in order to keep a basis set as close as possible to the extended one, and because only for the high spin state of the isolated atom are all $3d$ orbitals equivalent, and thus have the same radial part. One obtains in this minimal basis set a t_{2g} splitting of

$$\Delta E = \varepsilon(a_{1g}) - \varepsilon(e_g') = 41\ \text{meV}.$$

At this point we computed the effective orbital energies in only the crystalline field conditions; however, the result is still reversed from what is usually admitted within this approximation. Indeed, the Co^{4+} ion was computed in the sole electrostatic field of the NNOs, treated as -2 point charges; and the calculation is done within a minimal basis set and at the average CASSCF level.

F. Further analysis

In order to understand this puzzling result, we plotted the whole curve $\Delta E(\theta)$ (see Fig. 4) at this level of calculation and analyzed separately all energetic terms involved in this effective orbital energy difference.

One sees on Fig. 4 that the $\Delta E(\theta)$ curve is not monotonic, as expected from the crystalline field theory. Indeed, while for $\theta=0$ the relative order between the a_{1g} and e_g' orbitals is in agreement with the crystalline field predictions, for $\theta=90°$ the order is reversed. One should also notice that, in addition to the θ_0 value of the regular octahedron, there is another value of θ for which the three t_{2g} orbitals are degenerate. In the physically realistic region of the trigonal distortion (around the regular octahedron θ_0 value), the relative order between the a_{1g} and e_g' orbitals is reversed compared to the crystalline field predictions.

Let us now decompose $\Delta E(\theta)$ into its two-electron part within the $3d$ shell, $\Delta E_2(\theta)$, and the rest, referred to as the $3d$ single-electron part, $\Delta E_1(\theta)$. ΔE_1 includes the kinetic energy, the electron-nucleus and electron-charge interactions, and the interaction of the $3d$ electrons with the inner shell electrons.

One thus has

$$\Delta E = \Delta E_1 + \Delta E_2 = \varepsilon(a_{1g}) - \varepsilon(e_{g1}') = \varepsilon(a_{1g}) - \varepsilon(e_{g2}')$$

with

$$\Delta E_1 = \left\langle a_{1g} \middle| -\frac{\nabla^2}{2} \middle| a_{1g} \right\rangle - \left\langle e_g' \middle| -\frac{\nabla^2}{2} \middle| e_g' \right\rangle \tag{1}$$

$$+ \left\langle a_{1g} \middle| \sum_N \frac{-Z_N}{R_N} \middle| a_{1g} \right\rangle - \left\langle e_g' \middle| \sum_N \frac{-Z_N}{R_N} \middle| e_g' \right\rangle \tag{2}$$

$$\begin{aligned} &+ \sum_{\chi\ \text{occ}} 2\left\langle a_{1g}\chi \middle| \frac{1}{r_{12}} \middle| a_{1g}\chi \right\rangle \\ &- \left\langle a_{1g}\chi \middle| \frac{1}{r_{12}} \middle| \chi a_{1g} \right\rangle - \sum_{\chi\ \text{occ}} 2\left\langle e_g'\chi \middle| \frac{1}{r_{12}} \middle| e_g'\chi \right\rangle \\ &- \left\langle e_g'\chi \middle| \frac{1}{r_{12}} \middle| \chi e_g' \right\rangle \end{aligned} \tag{3}$$

and

$$\begin{aligned} \Delta E_2 = &\left\langle a_{1g}a_{1g} \middle| \frac{1}{r_{12}} \middle| a_{1g}a_{1g} \right\rangle - \left\langle e_g'e_g' \middle| \frac{1}{r_{12}} \middle| e_g'e_g' \right\rangle \\ &+ 2\left\langle a_{1g}e_g' \middle| \frac{1}{r_{12}} \middle| a_{1g}e_g' \right\rangle - \left\langle a_{1g}e_g' \middle| \frac{1}{r_{12}} \middle| e_g'a_{1g} \right\rangle \\ &- 2\left\langle e_{g1}'e_{g2}' \middle| \frac{1}{r_{12}} \middle| e_{g1}'e_{g2}' \right\rangle + \left\langle e_{g1}'e_{g2}' \middle| \frac{1}{r_{12}} \middle| e_{g2}'e_{g1}' \right\rangle, \end{aligned} \tag{4}$$

where the equations are given in atomic units. Z_N refers to the nuclear charge of the cobalt atom and the -2 point charges located at the NNO positions. R_N is the associated electron-charge distance. The sum on χ runs over all the orbitals of the cobalt inner shells.

Let us now examine the dependence on θ of each of the terms of ΔE_1 and ΔE_2.

Kinetic energy. The radial part of each of the $3d$ orbitals being identical due the the minimal basis set restriction, the kinetic part is identical for all $3d$ orbitals and thus its contribution to ΔE_1 (terms labeled 1 of ΔE_1) vanishes.

Nuclear interaction. Obviously this contribution to ΔE_1

(terms labeled 2 of ΔE_1) strongly depends on θ through the position of the -2 charges.

Interaction with the inner-shell electrons. This term (terms labeled 3 of ΔE_1) depends only on the shape of the t_{2g} and inner-shell orbitals. However, the minimal basis set does not leave any degree of freedom for the relaxation of the inner-shell orbital whose shapes are thus independent of θ. Similarly, the $3d$ radial part of the $3d$ orbitals is totally frozen.

ΔE_2. Finally, the dependence of ΔE_2 can only go through the shape of the a_{1g} and e_g' orbitals, whose radial part is totally frozen due to the use of a minimal basis set.

If one accepts that the a_{1g} and e_g' orbitals come from the t_{2g} orbitals of the regular octahedron, their angular form is totally given by the symmetry [see Eqs. (5) and (6)] and both ΔE_2 and the third contribution to ΔE_1 should be independent of θ:

$$e_g \begin{cases} e_{g1}^0 = \dfrac{1}{\sqrt{3}} d_{xy} + \dfrac{\sqrt{2}}{\sqrt{3}} d_{xz}, \\[2ex] e_{g2}^0 = \dfrac{1}{\sqrt{3}} d_{x^2-y^2} + \dfrac{\sqrt{2}}{\sqrt{3}} d_{yz}, \end{cases} \tag{5}$$

$$t_{2g} \begin{cases} a_{1g}^0 = d_{z^2}, \\[1ex] e_{g1}^{0\prime} = \dfrac{\sqrt{2}}{\sqrt{3}} d_{xy} - \dfrac{1}{\sqrt{3}} d_{xz}, \\[2ex] e_{g2}^{0\prime} = \dfrac{\sqrt{2}}{\sqrt{3}} d_{x^2-y^2} - \dfrac{1}{\sqrt{3}} d_{yz}, \end{cases} \tag{6}$$

where the x, y, and z coordinates are respectively associated with the **a**, **b**, and **c** crystallographic axes.

Figure 4 displays both ΔE_1 (dotted red curve) and ΔE_2 (dashed green curve) contributions to ΔE. One sees immediately that ΔE_2 is not at all independent of θ but rather monotonically increasing with θ. Thus the above hypothesis of the t_{2g} exclusive origin for the e_g' orbitals is not valid. Indeed, beyond the $\theta = \theta_0$ point, the only orbital perfectly defined by the symmetry is the a_{1g} orbital. The e_g' and e_g orbitals belong to the same irreducible representation (E_g) and can thus mix despite the large t_{2g}-e_g energy difference. If we name this mixing angle α, we have

$$e_{gi}' = e_{gi}^{0\prime} \cos\alpha + e_{gi}^0 \sin\alpha,$$

$$e_{gi} = -e_{gi}^{0\prime} \sin\alpha + e_{gi}^0 \cos\alpha.$$

Figure 5 displays α as a function of θ. One sees that the t_{2g}-e_g hybridization angle α is non-null—except for the regular octahedron—and a monotonically increasing function of θ. Even if very small (±0.6°), this t_{2g}-e_g hybridization has an important energetic effect, since it lowers the e_g' orbital energy while increasing the e_g one. α is very small but it modulates large energetic factors in ΔE_2: the on-site Coulomb repulsions of two electrons in the $3d$ orbitals. The result is a monotonically increasing variation of ΔE_2 as a function of θ. The variation of the ΔE_1 term is dominated by its nuclear interaction part and exhibits a monotonically decreasing variation as a function of θ, as expected from the crystalline field theory. The nuclear interaction and t_{2g}-e_g hybridization thus have opposite effects on the a_{1g}-e_g' splitting. The failure of the crystalline field theory thus comes from not considering the t_{2g}-e_g hybridization.

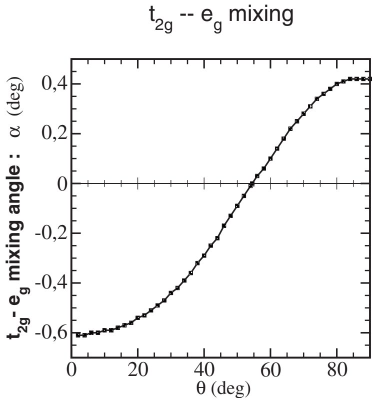

FIG. 5. t_{2g}-e_g hybridization angle under trigonal distortion.

In the calculations presented in Figs. 4 and 5, the screening effects on the on-site Coulomb repulsion and exchange integrals were not taken into account. Thus, the absolute value of ΔE_2 as a function of the hybridization α is very large and α is very small. When the screening effects are properly taken into account, the absolute value of ΔE_2 as a function of α is reduced by a factor of about 6, and the t_{2g}-e_g hybridization is much larger than the values presented in Fig. 5. Indeed, in the superconducting compound, for a realistic calculation including all effects, one finds $\alpha \simeq 13°$ ($\theta = 61.5°$).

At this point we would like to compare the a_{1g}-e_g' splitting found in the present calculations and the one found using DFT methods. Indeed, our splitting (315 meV for the superconducting compound) is larger than the DFT evaluations (always smaller than 150 meV). This point can be easily understood using the single-electron and two-electron partial analyses presented above. Indeed, while the single-electron part is perfectly treated in DFT calculations, the two-electron part is treated within the exchange-correlation kernel. However, these kernels are well known to fail to properly reproduce the strong correlation effects present in the transition metal open $3d$ shells. One thus expects that, while the single-electron part of the atomic orbital energies is well treated, the two-electron part is underestimated, resulting in an underevaluation of the a_{1g}-e_g' splitting, as can be clearly seen from Fig. 4. LDA+U and DMFT methods try to correct this point by introducing the on-site repulsion U. However, as can be seen in Eq. (4) the ΔE_2 term, responsible for the correct a_{1g}-e_g' splitting, is zero unless proper Racah's parameters are used, which is not the case in most calculations.

IV. OTHER CASES

We considered up to now a Co^{4+} ion, that is, five electrons in the $3d$ shell, and a fixed metal-ligand distance, $R_{M\text{-O}}$. Let us now examine the effect of the distance $R_{M\text{-O}}$ and the band filling on the a_{1g}-e_g' splitting. The calculations presented in

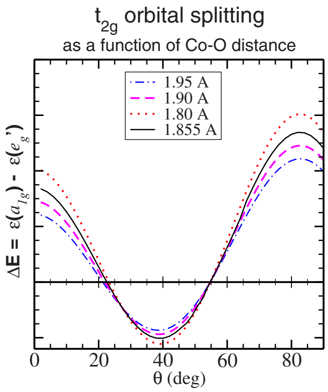

FIG. 6. (Color online) Orbital splitting between the a_{1g} and e_g' orbitals for a $3d^5$ transition metal and for different metal-ligand distances. Only the nearest-neighbor ligand electrostatic field is included in the calculation. The dotted red curve corresponds to $R_{\text{Co-O}}=1.8$ Å, the solid black curve corresponds to the superconducting compound ($R_{\text{Co-O}}=1.855$ Å), the dashed magenta curve corresponds to $R_{\text{Co-O}}=1.9$ Å, and finally the dot-dashed blue curve corresponds to $R_{\text{Co-O}}=1.95$ Å.

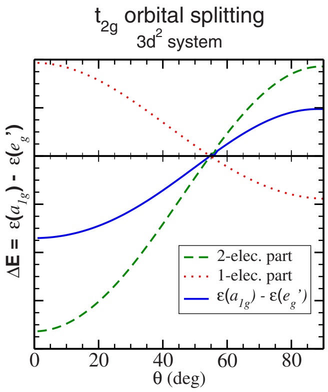

FIG. 7. (Color online) Orbital splitting between the a_{1g} and e_g' orbitals for a $3d^2$ transition metal. Only the nearest-neighbor ligand electrostatic field is included in the calculation. The dotted red curve corresponds to the single-electron part of the orbital energy difference, ΔE_1, that is, the kinetic energy [Eq. (1)], the electron-charge interaction [Eq. (2)], and the interaction with the core electrons [Eq. (3)]. The dashed green curve corresponds to the two-electron part of the orbital energy difference, ΔE_2, that is, the repulsion and exchange terms within the $3d$ shell [Eq. (4)].

this section follow the same procedure as in Secs. III E and III F. For different fillings a typical example in the transition metal oxide family was used to define the type of metallic atom and metal oxygen distances. The minimal basis set coming from full contraction of the basis set given in Ref. 11 will be used.

A. The effect of the Co-O distance

Figure 6 displays the a_{1g}-e_g' energy splitting as a function of the distortion angle θ and for different distances. The range of variation, from 1.8 to 1.95 Å, includes all physically observed distances in CoO_2 layers.

One sees immediately that, despite the large variation of the metal-ligand distance, the relative order of the a_{1g} and e_g' orbitals remains identical. The main effect of $R_{M\text{-O}}$ is thus to renormalize the amplitude of the splitting, lowering the splitting for larger distances and increasing it for smaller ones.

B. $3d^1$

The simplest filling case corresponds to only one electron in the $3d$ shell. This is, for instance, the case of the $NaTiO_2$ compound. The calculations were done using the average Ti-O distance found in $NaTiO_2$,[13] $R_{\text{Ti-O}}=2.0749$ Å.

In this case, $\Delta E_2=0$ and $\Delta E(\theta)=\Delta E_1(\theta)$ behaves as pictured in Fig. 4. The a_{1g} orbital is of lower energy than the e_g' for $\theta>\theta_0$ and of higher energy for $\theta<\theta_0$. This result is in perfect agreement with crystalline field theory.

C. $3d^2$

A simple example of $3d^2$ filling in transition metal oxides is the $LiVO_2$ compound. Indeed, the vanadium atom is in the V^{3+} ionization state. We thus used a metal-oxygen distance of $R_{\text{V-O}}=1.9787$ Å.[14] Figure 7 displays the a_{1g}-e_g' splitting as well as its decomposition into the single-electron and two-electron parts.

As in the $3d^5$ case (Fig. 4), the single-electron and two-electron parts behave in a monotonic way as a function of θ, and in an opposite manner. In the present case, however, the two-electron part always dominates over the one-electron part, and the a_{1g}-e_g' orbital splitting is always reversed compared to the crystalline field predictions. As for the $3d^5$ system, there is a slight e_g'-e_g hybridization that is responsible for the t_{2g} orbital order.

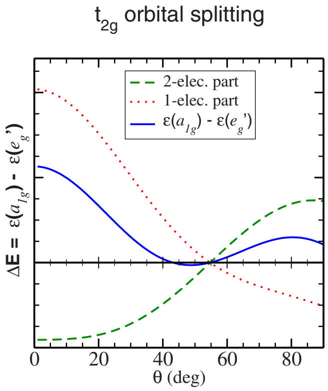

FIG. 8. (Color online) Orbital splitting between the a_{1g} and e_g' orbitals for a $3d^3$ transition metal. Only the nearest-neighbor ligand electrostatic field is included in the calculation. The dotted red curve corresponds to the single-electron part of the orbital energy difference, ΔE_1, that is, the kinetic energy [Eq. (1)], the electron-charge interaction [Eq. (2)], and the interaction with the core electrons [Eq. (3)]. The dashed green curve corresponds to the two-electron part of the orbital energy difference, ΔE_2, that is, the repulsion and exchange terms within the $3d$ shell [Eq. (4)].

D. $3d^3$

Examples of $3d^3$ transition metal oxides are found easily in the chromium compounds. Let us take for instance the $NaCrO_2$ system.[15] The metal oxygen distance is thus $R_{\text{Cr-O}} \simeq 1.901$ Å. Figure 8 displays the a_{1g}-e_g' orbital splitting as well as its decomposition into single- and two-electron parts.

As usual the single-electron part and the two-electron part are monotonic as functions of θ but with slopes of opposite signs. This case is quite similar to the $3d^5$ case since neither of the single- and two-electron parts dominates the t_{2g} orbital splitting over the whole range. Indeed, for small values of θ, the crystalline field effect dominates and the a_{1g} orbital is above the e_g' ones while, for large values of θ, the two-electron part dominates and the a_{1g} orbital is again above the e_g' ones. In a small intermediate region the order is reversed. In the realistic range of θ ($\theta \simeq \theta_0$) there is a strong competition between the two effects (quasidegeneracy of the a_{1g} and e_g' orbitals) and no simple theoretical prediction can be made. The crystalline field theory is not predictive but the present calculations cannot be considered as predictive either, since all the neglected effects may reverse the a_{1g}-e_g' order.

V. DISCUSSION AND CONCLUSION

In the present work we studied the validity of the crystalline field theory under the application of a trigonal distortion on the regular octahedron. Under such a distortion, the T_{2g} irreducible representation (irrep) of the O_h group spits into A_{1g} and E_g irreps ($T_{2g} \rightarrow A_{1g} \oplus E_g$), while the e_g irrep remains untouched ($E_g \rightarrow E_g$). The hybridization between the t_{2g} and e_g orbitals thus becomes symmetry allowed, even if hindered by energetic factors. This hybridization is not taken into account in the crystalline field theory. It is, however, of crucial importance for the relative order between the former t_{2g} orbitals and the reason for the failure of the crystalline field theory to be predictive. Indeed, due to the t_{2g}-e_g orbital hybridization, the two-electron part of the e_g' orbital energy becomes dependent on the amplitude of the distortion and of opposite effect to that of the single-electron part. The relative order of the t_{2g} orbitals thus depends on the competition between these two effects and as a consequence of the band filling.

In this work we studied the O_h to D_{3d} distortion; however, one can expect similar effects to take place for other distortions of the regular octahedron. The condition for these effects to take place is that the T_{2g} irreducible representation splits into a one-dimensional irrep (A) and the same two-dimensional irrep (E) as the one the e_g orbitals are transformed to:

$$T_{2g} \rightarrow A \oplus E,$$

$$E_g \rightarrow E.$$

Indeed, under such a distortion, t_{2g}-e_g hybridization phenomena are allowed. The distortion should thus transform O_h into subgroups that keep the C_3 (111) symmetry axis: C_3, C_{3v}, D_3, S_6, and D_{3d}. Examples of such deformations are the elongation of the metal-ligand distance of one of the sets of three symmetry-related ligands, or the rotation of such a set of three ligands around the (111) symmetry axis. For instance, one expects that t_{2g}-e_g hybridization will also take place in trigonal prismatic coordination.

However, in real systems like the sodium cobaltites, these distortion do not usually appear alone but rather coupled. For instance, in the squeezing of the metal layer between the two oxygen layers observed as a function of the sodium content in Na_xCoO_2, the Co-O bond length and the threefold trigonal distortion are coupled. Since this composed distortion belongs to the above-cited class, t_{2g}-e_g hybridization will take place and the relative orbital order between the a_{1g} and e_g' orbitals will be qualitatively the same as in Fig. 4. The bond length modification at equal distortion angle θ will change only the quantitative value of the orbital splitting, but not its sign. Bond elongation reduces the splitting and bond compression increases it. One can thus expect in sodium cobaltites that the a_{1g}-e_g' orbital energy splitting will decrease with increasing sodium content. The reader should, however, keep in mind that the effects of this splitting reduction will remain relatively small compared to the bandwidth, as clearly seen in Ref. 16. In fact, one can expect that a large effect will be the modification of the band dispersion due not only to the bond length modification, but also to the t_{2g}-e_g hybridization.

ACKNOWLEDGMENTS

The authors thank Jean-Pierre Doumerc and Michel Pouchard for helpful discussions and Daniel Maynau for providing us with the CASDI suite of programs. These calculations were done using the CNRS IDRIS computational facilities under Project No. 1842.

---

[1] K. Takada, H. Sakurai, E. Takayama-Muromachi, F. Izumi, R. A. Dilanian, and T. Sasali, Nature (London) **422**, 53 (2003).

[2] I. Terasaki, Y. Sasago, and K. Uchinokura, Phys. Rev. B **56**, R12685 (1997).

[3] W. Koshibae and S. Maekawa, Phys. Rev. Lett. **91**, 257003 (2003).

[4] L.-J. Zou, J.-L. Wang, and Z. Zeng, Phys. Rev. B **69**, 132505 (2004).

[5] M. D. Johannes, I. I. Mazin, D. J. Singh, and D. A. Papaconstantopoulos, Phys. Rev. Lett. **93**, 097005 (2004).

[6] S. Landron and M.-B. Lepetit, Phys. Rev. B **74**, 184507 (2006).

[7] M. Z. Hasan, Y.-D. Chuang, D. Qian, Y. W. Li, Y. Kong, A. Kuprin, A. V. Fedorov, R. Kimmerling, E. Rotenberg, K. Rossnagel, Z. Hussain, H. Koh, N. S. Rogado, M. L. Foo, and R. J. Cava, Phys. Rev. Lett. **92**, 246402 (2004); H.-B. Yang, S.-C. Wang, A. K. P. Sekharan, H. Matsui, S. Souma, T. Sato, T. Takahashi, T. Takeuchi, J. C. Campuzano, R. Jin, B. C. Sales, D. Mandrus, Z. Wang, and H. Ding, *ibid.* **92**, 246403 (2004); H.-B.

Yang, Z.-H. Pan, A. K. P. Sekharan, T. Sato, S. Souma, T. Takahashi, R. Jin, B. C. Sales, D. Mandrus, A. V. Fedorov, Z. Wang, and H. Ding, *ibid.* **95**, 146401 (2005).

[8] M. B. Lepetit, *Recent Research Developments in Quantum Chemistry 3* (Transword Research Network, Trivandrum, India, 2002).

[9] B. O. Roos, P. R. Taylor, and P. E. Siegbahn, Chem. Phys. **48**, 157 (1980); B. O. Roos, *Advances in Chemical Physics; Ab Initio Methods in Quantum Chemistry II* (John Wiley & Sons, Chichester, England, 1987), Chap. 69, p. 399.

[10] J. Miralles, J. P. Daudey, and R. Caballol, Chem. Phys. Lett. **198**, 555 (1992); V. M. García *et al.*, *ibid.* **238**, 222 (1995); V. M. García, M. Reguero, and R. Caballol, Theor. Chem. Acc. **98**, 50 (1997).

[11] Z. Barandiaran and L. Seijo, Can. J. Chem. **70**, 409 (1992).

[12] N. W. Winter, R. M. Pitzer, and D. K. Temple, J. Chem. Phys. **86**, 3549 (1987).

[13] S. J. Clarke, A. J. Fowkes, A. Harrison, R. M. Ibberson, and M. J. Rosseinsky, Chem. Mater. **10**, 372 (1998).

[14] L. P. Cardoso, D. E. Cox, T. A. Hewston, and B. L. Chamberland, J. Solid State Chem. **72**, 234 (1988).

[15] W. Ruedorff and H. Becker, Z. Naturforsch. B **9**, 614 (1954).

[16] E. R. Ylvisaker, K. W. Lee, and W. E. Pickett, Physica B **383**, 53 (2006).